

# Type-II see-saw at $\mu^+\mu^-$ collider

Siddharth P. Maharathy<sup>1,2,\*</sup> and Manimala Mitra<sup>1,2,†</sup>

<sup>1</sup>*Institute of Physics, Bhubaneswar, Sachivalaya Marg, Sainik School, Bhubaneswar 751005, India*

<sup>2</sup>*Homi Bhabha National Institute, Training School Complex, Anushakti Nagar, Mumbai 400094, India*

Doubly-charged Higgs bosons have extensively been searched at the LHC. In this work, we study the sensitivity reach of the doubly-charged scalar ( $H^{\pm\pm}$ ) in muon collider for the well-known Type-II seesaw scenario. First, we perform a cut-based analysis to predict the discovery prospect in the muon collider operating with 3 TeV center of mass energy. In addition to this, we have also performed a multivariate analysis and compare the cut-based result with the result obtained from the multivariate analysis. We find that the cut-based analysis is more significant as compared to the multivariate analysis in the large doubly-charged scalar mass region. We predict that a doubly-charged scalar mass,  $M_{H^{\pm\pm}}$ , upto 1450 GeV can be probed with  $5\sigma$  significance for center of mass  $\sqrt{s} = 3$  TeV and integrated luminosity  $\mathcal{L} = 1000 \text{ fb}^{-1}$ .

## I. INTRODUCTION

The discovery of the Higgs boson at the Large Hadron Collider (LHC) assured the Brout-Englert-Higgs (BEH) mechanism to be the most accurate formalism responsible for the generation of the Standard Model (SM) fermions and gauge-bosons masses. The BEH mechanism can generate Dirac mass for neutrino by extending the SM with right-handed neutrinos, however, to explain eV scale small neutrino masses, a very tiny Yukawa  $10^{-12}$  is required, enhancing the fine-tuning problem of the SM to a multi-fold level. One of the most appealing mechanisms to describe tiny neutrino mass is via seesaw, where light neutrino masses are generated from higher dimensional  $d = 5$  Weinberg operator [1].

The tree level realization of the Weinberg operator are Type-I [2–5], Type-II [5–7] and Type-III [8] seesaw mechanisms, where the SM has been extended with a  $SU(2)_L$  singlet fermion,  $SU(2)_L$  triplet scalar with hyper-charge  $Y = 1$  and a  $SU(2)_L$  triplet fermion with hyper-charge  $Y = 0$  respectively. Among these, in the second variant of the seesaw mechanism, referred as the Type-II seesaw, generated light neutrino mass is proportional to the  $vev$  of the triplet scalar folded with the respective Yukawa coupling.

Since the triplet scalar has gauge coupling, hence it can be produced abundantly and then decays to SM particles. Depending on the triplet  $vev$  the doubly-charged scalars can decay to same-sign di-lepton, same-sign gauge bosons

and can also decay through cascade decay. The phenomenology of the doubly-charged scalar has extensively been studied for LHC [9–42],  $e^+e^-$  [43–48] collider and also for  $ep$  machine [49–52]. Several searches have been performed at the LHC by both ATLAS and CMS collaboration, and the lack of any excess from the SM signal imposes stringent bounds on the parameter space [53–63]. The ATLAS multi lepton search [58] sets a limit of 770–870 GeV and 450 GeV on the mass of  $H^{\pm\pm}$  considering  $B(H^{\pm\pm} \rightarrow l^\pm l^\pm) = 100\%$  and  $B(H^{\pm\pm} \rightarrow l^\pm l^\pm) = 10\%$  respectively. Taking into account the  $W^\pm W^\pm$  or  $W^\pm Z$  decay mode of the charged scalars, the ATLAS search [62] excludes  $H^{\pm\pm}$  in the range 200–350 GeV and 230 GeV, for pair and associated production modes. For  $3000 \text{ fb}^{-1}$  luminosity, with the aforementioned decay mode of the charged scalars, expected reach of the doubly-charged scalar increases up to 640 GeV [41]. The most stringent bound from CMS is from the CMS multilepton search [60], limiting  $H^{\pm\pm}$  mass to 535–820 GeV. With the assumption of equal branching ratios to each possible leptonic final states,  $Br(H^{\pm\pm} \rightarrow e^\pm e^\pm) = Br(H^{\pm\pm} \rightarrow e^\pm \mu^\pm) = Br(H^{\pm\pm} \rightarrow e^\pm \tau^\pm) = Br(H^{\pm\pm} \rightarrow \mu^\pm \mu^\pm) = Br(H^{\pm\pm} \rightarrow \mu^\pm \tau^\pm) = Br(H^{\pm\pm} \rightarrow \tau^\pm \tau^\pm)$ , the ATLAS multi-lepton search [63] imposes a lower limit of 1080 GeV on doubly charged scalars mass.

Other than a  $pp$  machine, the doubly-charged Higgs can also be searched at future lepton colliders: Linear or Circular electron positron collider [64–67] and muon colliders [68–72]. For higher TeV scale masses of the doubly charged Higgs for which cross-section at the LHC is  $\sim \mathcal{O}(\text{fb})$  or even lower, and to probe hadronic final states, lepton collider can be most useful, as depending upon the centre of mass energy, the cross-section for dou-

\* siddharth.m@iopb.res.in

† manimala@iopb.res.in

bly charged Higgs production is typically large until the kinematic threshold. Additionally, a lepton collider can be more effective because of its cleaner signal. In case of muon collider the collision is free from any pile-up events. An additional benefit is, contrary to the circular  $e^+e^-$  colliders, a muon collider suppresses the loss of energy due to synchrotron radiation because of the heavier mass of muon, thereby making both high energy as well as high luminosity achievable. In this work we choose a particular configuration of muon collider: center-of-mass energy ( $\sqrt{s}$ ) = 3 TeV and integrated luminosity ( $\mathcal{L}$ ) = 1000 fb $^{-1}$  and explore the sensitivity reach for the doubly charged scalar. Some recent works on BSM particle searches at muon collider can be found in [73–75].

The paper is arranged in the following way. In Sec. [II] we discuss the model description of Type-II seesaw. We discuss the collider analysis that includes both the cut based as well as multivariate analysis in Sec. [III]. Finally in Sec. [IV] we summarize our outcomes.

## II. MODEL

The Type-II seesaw model has an extended scalar sector, where in addition to the SM scalar doublet,  $\Phi = (\Phi^+ \ \Phi^0)^T$ , a  $SU(2)$  triplet scalar with hyper-charge  $Y=1$  is also present.

$$\Delta = \begin{pmatrix} \frac{\Delta^+}{\sqrt{2}} & \Delta^{++} \\ \Delta^0 & -\frac{\Delta^+}{\sqrt{2}} \end{pmatrix} \quad (1)$$

The neutral components of the scalars are parameterised as  $\Phi^0 = (v_\Phi + \phi^0 + iZ_1)/\sqrt{2}$  and  $\Delta^0 = (v_\Delta + \delta^0 + iZ_2)/\sqrt{2}$ . The vacuum expectation values (*vevs*) of the SM doublet and the BSM triplet are  $v_\Phi$  and  $v_\Delta$  respectively, and they satisfy the relation  $v = \sqrt{v_\Phi^2 + 2v_\Delta^2} = 246$  GeV.

The kinetic Lagrangian of the SM scalar doublet  $\Phi$  and the scalar triplet  $\Delta$  has the following form,

$$\mathcal{L}_{\text{kin}}(\Phi, \Delta) = (D_\mu \Phi)^\dagger (D^\mu \Phi) + \text{Tr}[(D_\mu \Delta)^\dagger (D^\mu \Delta)] . \quad (2)$$

In the above, the covariant derivatives are given by,

$$\begin{aligned} D_\mu \Phi &= \left( \partial_\mu + i\frac{g}{2}\tau^a W_\mu^a + i\frac{g'}{2}B_\mu \right) \Phi , \\ D_\mu \Delta &= \partial_\mu \Delta + i\frac{g}{2}[\tau^a W_\mu^a, \Delta] + ig' B_\mu \Delta . \end{aligned} \quad (3)$$

The scalar potential of the model is,

$$\begin{aligned} V(\Phi, \Delta) &= -m_\Phi^2 \Phi^\dagger \Phi + \tilde{M}_\Delta^2 \text{Tr}(\Delta^\dagger \Delta) \\ &+ (\mu \Phi^T i\tau_2 \Delta^\dagger \Phi + \text{h.c.}) + \frac{\lambda}{4}(\Phi^\dagger \Phi)^2 \\ &+ \lambda_1(\Phi^\dagger \Phi) \text{Tr}(\Delta^\dagger \Delta) + \lambda_2 [\text{Tr}(\Delta^\dagger \Delta)]^2 \\ &+ \lambda_3 \text{Tr}[(\Delta^\dagger \Delta)^2] + \lambda_4 \Phi^\dagger \Delta \Delta^\dagger \Phi . \end{aligned} \quad (4)$$

After the symmetry breaking the charged scalars and neutral scalars mix resulting several physical mass eigenstates. The masses can be obtained by diagonalising with rotation matrices,  $R^\pm$ ,  $R^0$  and  $R_A^0$ , respectively:

$$R^\pm = \begin{pmatrix} c_{\beta_\pm} & -s_{\beta_\pm} \\ s_{\beta_\pm} & c_{\beta_\pm} \end{pmatrix}, R^0 = \begin{pmatrix} c_{\beta_0} & -s_{\beta_0} \\ s_{\beta_0} & c_{\beta_0} \end{pmatrix} \quad (5)$$

$$R_A^0 = \begin{pmatrix} c_\alpha & -s_\alpha \\ s_\alpha & c_\alpha \end{pmatrix} \quad (6)$$

where  $c_{\beta_\pm} = \cos \beta_\pm$ ,  $c_{\beta_0} = \cos \beta_0$ ,  $c_\alpha = \cos \alpha$ . The mixing angles  $\beta_\pm$ ,  $\beta_0$  and  $\alpha$  have the following forms:

$$\sqrt{2} \tan \beta_\pm = \tan \beta_0 = \frac{2v_\Delta}{v_\Phi}, \quad \tan 2\alpha = \frac{2B}{A-C} \quad (7)$$

where  $A = \frac{\lambda v_\Phi^2}{2}$ ,  $B = -\sqrt{2}\mu v_\Phi + (\lambda_1 + \lambda_4)v_\Phi v_\Delta$  and  $C = \frac{\mu v_\Phi^2}{\sqrt{2}v_\Delta} + 2(\lambda_2 + \lambda_3)v_\Delta^2$ . In the above  $R^\pm$  represents the rotation matrix between charged scalar eigenstates,  $R^0, R_A^0$  represent the rotation matrix between the CP-even and CP-odd neutral scalar states, respectively.

In addition to the three Goldstone bosons  $G^\pm$  and  $G^0$  which give masses to the gauge bosons, there are seven physical mass eigen states  $H^{\pm\pm}$ ,  $H^\pm$ ,  $A$ ,  $H$  and  $h$ . The gauge basis and mass basis for these scalar states are related as,

$$\begin{aligned} \begin{pmatrix} \Phi^\pm \\ \Delta^\pm \end{pmatrix} &= R^\pm \begin{pmatrix} G^\pm \\ H^\pm \end{pmatrix}, \quad \begin{pmatrix} Z_1^0 \\ Z_2^0 \end{pmatrix} = R_A^0 \begin{pmatrix} G^0 \\ A \end{pmatrix} \\ \begin{pmatrix} \phi^0 \\ \delta^0 \end{pmatrix} &= R^0 \begin{pmatrix} h \\ H \end{pmatrix}. \end{aligned} \quad (8)$$

A detailed discussion on the mass spectrum of the physical scalars of the model has been presented in [76]. With the assumption:  $v_\Delta \ll v_\Phi$ , the masses of the physical scalars takes the following simplified form,

$$\begin{aligned} M_{H^{\pm\pm}}^2 &\simeq \tilde{M}_\Delta^2 - \frac{\lambda_4}{2}v_\Phi^2, \quad M_{H^\pm}^2 \simeq \tilde{M}_\Delta^2 - \frac{\lambda_4}{4}v_\Phi^2, \\ M_h^2 &\simeq 2v_\Phi^2\lambda, \quad M_H^2 \approx M_{\tilde{H}}^2 \simeq \tilde{M}_\Delta^2 \end{aligned}$$

where  $\tilde{M}_\Delta^2 \equiv \frac{\mu v_\Phi^2}{\sqrt{2} v_\Delta}$  and the mass-squared differences are obtained as,

$$M_{H^\pm}^2 - M_{H^{\pm\pm}}^2 \approx M_{H,A}^2 - M_{H^\pm}^2 \approx \frac{\lambda_4}{4} v_\Phi^2 \quad (9)$$

Considering the sign of  $\lambda_4$ , three possible mass spectrum of the physical scalars can be realised,

(i) Degenerate scenario ( $\lambda_4 = 0$ ):  $M_{H^{\pm\pm}}^2 = M_{H^\pm}^2 = M_{H,A}^2$

(ii) Normal scenario ( $\lambda_4 > 0$ ):  $M_{H^{\pm\pm}}^2 > M_{H^\pm}^2 > M_{H,A}^2$

(iii) Inverted scenario ( $\lambda_4 < 0$ ):  $M_{H^{\pm\pm}}^2 < M_{H^\pm}^2 < M_{H,A}^2$

The Yukawa interaction of the model responsible for neutrino mass is,

$$-\mathcal{L} = Y_{ij} L_i^T C i \sigma_2 \Delta L_j + h.c. \quad (10)$$

where  $Y$  is a  $3 \times 3$  complex symmetric matrix and  $L = (\nu_L, l_L)^T$  is the left-handed SM lepton doublet. After the triplet scalar,  $\Delta$ , acquires the  $vev$  ( $v_\Delta$ ), a tiny neutrino mass can be obtained from Yukawa term in Eq. 10 as,

$$m_\nu = \sqrt{2} Y v_\Delta \quad (11)$$

The above  $3 \times 3$  matrix,  $m_\nu$ , can further be diagonalised by unitary transformation by Pontecorvo-Maki-Nakagawa-Sakata (PMNS) matrix  $U_{PMNS}$  as  $U_{PMNS}^T m_\nu U_{PMNS} = m_\nu^d = \text{diag}(m_1, m_2, m_3)$ , where  $m_1, m_2, m_3$  are the three mass eigen values. The matrix  $U_{PMNS}$  is parameterized by three mixing angles ( $\theta_{12}, \theta_{23}, \theta_{13}$ ), one Dirac phase ( $\delta$ ) and two Majorana phases ( $\phi, \phi'$ ).

Various constraints on the model parameter space are the following,

- *Constraints from electroweak precision data (EWPD):* The  $\rho$ -parameter ( $m_W^2/m_Z^2 \cos^2 \theta_W$ ) of the model in terms of the doublet and triplet  $vev$  is defined as [40, 41],

$$\rho = (v_\Phi^2 + 2v_\Delta^2)/(v_\Phi^2 + 4v_\Delta^2)$$

the present *EWPD* [77] sets the value of  $\rho$  parameter as,  $\rho = 1.00038(20)$  which is  $1.9\sigma$  away from SM tree-level value ( $\rho = 1$ ) and this leads to an upper bound of  $\mathcal{O}(1)$  GeV on  $v_\Delta$ .

- *Constraints from oblique parameters:* The mass splitting,  $\Delta m$ , between the different physical scalars affects the *EWPD* observable, named as oblique parameters ( $S$ ,  $T$  and  $U$  parameters). These parameters constraints the mass splitting as  $\Delta m < 40$  GeV [9, 24].
- *Constraints from lepton flavour violation(LFV):* From the Yukawa interaction shown in Eq. 10, *LFV* decays like  $\mu \rightarrow e\gamma$  at loop-level and  $\mu \rightarrow 3e$  at tree-level can be possible. The branching fractions can be calculated as [78, 79],

$$BR(\mu \rightarrow e\gamma) = \frac{\alpha |(Y^\dagger Y)_{e\mu}|^2}{192\pi G_F^2} \left( \frac{1}{m_{H^\pm}^2} + \frac{8}{m_{H^{\pm\pm}}^2} \right)$$

$$BR(\mu \rightarrow 3e) = \frac{|(Y_{ee}^\dagger Y_{\mu e})|^2}{4G_F^2 m_{H^{\pm\pm}}^4}$$

where  $\alpha$  is the electromagnetic fine-structure constant and  $G_F$  is the Fermi constant. The upper bounds on the above processes,  $4.2 \times 10^{-13}$  for  $\mu \rightarrow e\gamma$  [80] and  $1.0 \times 10^{-12}$  for  $\mu \rightarrow 3e$  [81] limit the lower value of the triplet  $vev(v_\Delta)$ , which can be expressed as [41],

$$v_\Delta \gtrsim 0.78 - 1.5(0.69 - 2.3) \text{ GeV} \times 10^{-9} \times \frac{1 \text{ TeV}}{M_{H^{\pm\pm}}}$$

for NH(IH).

- *Constraints from Colliders:* For  $\Delta m = 0$  with large(small)  $v_\Delta$ , doubly-charged scalar mass below 420(955) GeV has already been excluded [41]. The limit extends upto 1115 GeV for  $\Delta m < 0$  and moderate  $v_\Delta$ . However for moderate  $v_\Delta$  with  $\Delta m > 0$ , doubly-charged scalar as light as 200 GeV are still allowed by the LHC results.

## A. Decay Widths and Branching Ratios

In this section, we discuss the different decay modes of the scalars:  $H^{\pm\pm}$ ,  $H^\pm$ ,  $A$  and  $H$ . We are mainly inter-

ested on the degenerate mass spectrum of these scalars and hence we have not given much attention to the other mass spectrums (Normal and Inverted scenario). The decay width of the scalars are extensively studied and can

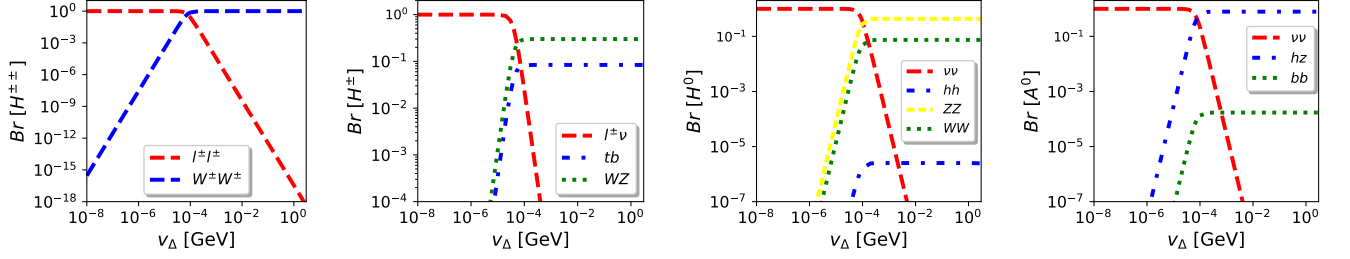


FIG. 1. Branching ratios of doubly-charged scalar:  $H^{\pm\pm}$  (left panel), singly-charged scalar:  $H^{\pm}$  (2nd panel), CP-even scalar:  $H$  (3rd panel) and CP-odd scalar:  $A$  (right panel) versus triplet  $vev$  ( $v_{\Delta}$ ) for an illustrative benchmark point  $M_{H^{\pm\pm}} = M_{H^{\pm}} = M_H = M_A = 1000$  GeV.

be found in [17, 20, 82–84]. In Fig. 1, we have shown the branching fractions of all the aforementioned scalars having a degenerate mass of 1000 GeV. From the figure it is quite evident that for  $v_{\Delta} < 10^{-4}$  GeV, all the scalars dominantly decay into leptonic final states ( $l^{\pm}l^{\pm}$ ,  $l^{\pm}\nu$  and  $\nu\nu$ ). However, for  $v_{\Delta} > 10^{-4}$  GeV the hadronic decay modes ( $t\bar{t}$ ,  $t\bar{t}$  and  $b\bar{b}$ ) along with the di-boson decay modes ( $WW$ ,  $WZ$ ,  $hZ$  and  $hh$ ) starts to dominate over the leptonic decay mode.

When the non-degenerate scenario is realized, *viz*  $\Delta m \neq 0$ , cascade decay modes turn out to be important. This scenario is beyond the scope of our work, however the interested readers can look for this scenario in [41].

### III. COLLIDER ANALYSIS

In this section, we discuss the potential strength of  $\mu^+\mu^-$  collider in probing doubly-charged scalars and exploring its sensitivity reach mainly in the high mass regime. A center of mass energy of  $\sqrt{s} = 3$  TeV is being considered for our collider analysis. The overall analysis is focused mainly in the large triplet  $vev$  region,  $v_{\Delta} > 10^{-4}$ , where the gauge boson mode of the doubly-charged scalars is dominant. At muon collider the doubly-charged scalars,  $H^{\pm\pm}$ , is produced by photon and  $Z$  mediated Drell–Yan (DY) processes, shown in Fig. 4. The DY pair production cross section of the doubly-charged scalars has been shown in Fig. 2 for two different configuration of muon colliders,  $\sqrt{s} = 3$ , and 6 TeV along with the production cross section at 13 TeV LHC. Being an s-channel process the production cross section decreases with the increase in center-of-mass energy. A sharp fall in the production cross section can be seen around the kinematic threshold of each configurations of muon collider i.e. around  $M_{H^{\pm\pm}} \sim \frac{\sqrt{s}}{2}$ . As can be seen from

the figure that after  $\mathcal{O}(400)$  GeV mass range, clearly the cross-section in the muon collider is substantially large. In the following analysis we mainly focus into the multi jet final state resulting from the decay of  $H^{\pm\pm}$ , as all hadronic final state in a leptonic collider can provide a better sensitivity reach.

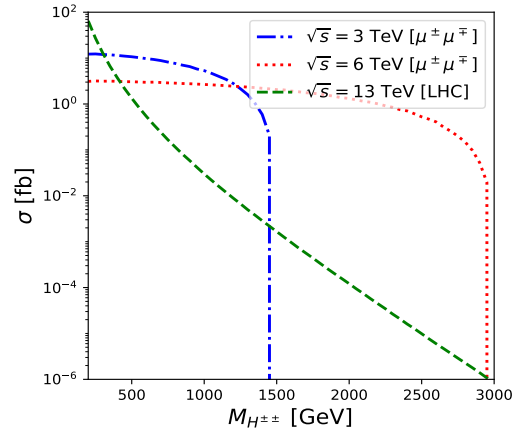


FIG. 2. Production cross-section of doubly-charged scalars ( $H^{\pm\pm}$ ) as a function of  $M_{H^{\pm\pm}}$  for 3, and 6 TeV  $\mu^+\mu^-$  collider along with 13 TeV LHC.

#### A. Multijet signature

The analysis in the paper aim to probe the high  $v_{\Delta}$  regime of the parameter space, the region dominated by the gauge production of  $H^{\pm\pm}$  and its subsequent decay into multijet final states. The parameter space of our interest is the higher mass region of  $H^{\pm\pm}$  where the production of  $W^{\pm}$  is on-shell. In this region the jets resulted from  $W^{\pm}$  are highly collimated, and fat-jets reconstruction is more favorable. Thus our signal comprises of up to

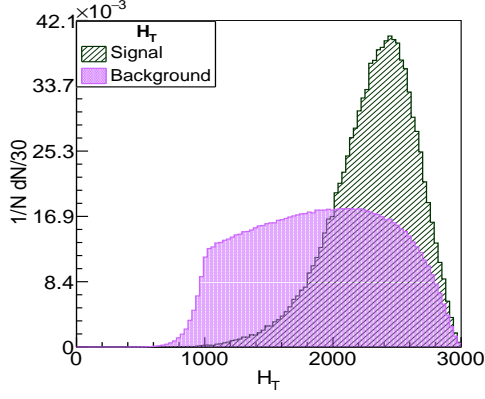


FIG. 3. Normalized  $H_T$  distribution for signal (benchmark point  $M_{H^{\pm\pm}} = 1$  TeV) and background at 3 TeV  $\mu^+\mu^-$  collider.

4 fat-jets as shown in the Fig. 4. The production process for this signal is,

$$\mu^+\mu^- \rightarrow H^{\pm\pm} H^{\mp\mp} \rightarrow 4W^{\pm} (W^{\pm} \rightarrow jj) \quad (12)$$

A significant number of SM background can mimic these

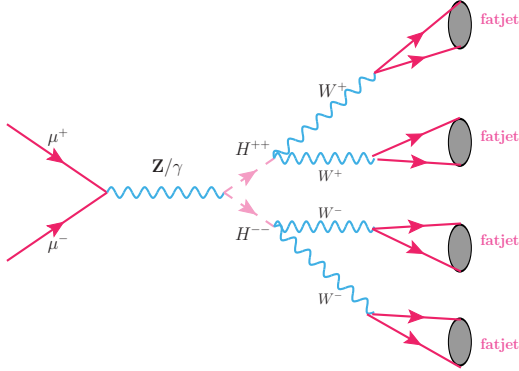


FIG. 4. The Feynman diagram for pair production of doubly-charged scalars ( $H^{\pm\pm}$ ) via Drell-Yan process and their consecutive decays leading to multijet final state.

final states with multiple fat-jets. We consider the following sets of backgrounds in our analysis,

$$\begin{aligned} \mu^+\mu^- &\rightarrow jjjj \\ \mu^+\mu^- &\rightarrow V + 2j \quad (V \rightarrow jj) \\ \mu^+\mu^- &\rightarrow V + 3j \quad (V \rightarrow jj) \\ \mu^+\mu^- &\rightarrow VV + 2j \quad (V \rightarrow jj) \\ \mu^+\mu^- &\rightarrow VVV + 2j \quad (V \rightarrow jj) \end{aligned} \quad (13)$$

where  $V = (W^{\pm}, Z, h)$ .

MadGraph5aMC@NLO [85] is used to generate parton level signal and background processes. During the generation process some pre-selection cuts have been implemented to reduce the size of the background. The following enumerated points discuss about these pre-selection cuts,

- (i) Since the signal contains at-least 4-jets (fat-jets) we imposed an increased jet-jet separation criteria at the production level, mainly for 4j background. The 4j background is generated with  $\Delta R(j, j) > 0.6$  and  $p_T^j > 60$  GeV. The  $p_T$  requirement is only on the leading 4-jets and the rest of the jets are required to have relaxed minimum  $p_T$  value i.e.  $p_T \geq 20$  GeV. For all other background processes the jet-jet separation is  $\Delta R(j, j) > 0.4$  and the leading 4-jets have a minimum  $p_T$  value,  $p_T^j > 60$  GeV. The minimum  $p_T$  requirement on the background processes is justified, as most of the signal is mainly populated in the high  $p_T$  region, as can be seen from Fig. 5.
- (ii) Fig. 3 corresponds to scalar sum of transverse momenta of all visible objects,  $H_T$ , of both signal and backgrounds. Most of the signals are populated at high  $H_T$  region as compared to the background. Hence we have also imposed a minimum  $H_T$  criteria of  $H_T > 1000$  GeV on all the background processes at the generation level i.e. during the production of backgrounds at Madgraph.

After the parton level event generation in MadGraph5aMC@NLO [85], we then pass the generated events into Pythia8 [86] for showering and hadronization. For simulating detector effects we use Delphes3 [87], and reconstructed jets, electrons, muons and missing energy ( $E_T^{miss}$ ). The purpose is accomplished by using the Delphes ILD card. We use FastJet [88] for the clustering of jets and consider Cambridge-Aachen (CA) jet clustering algorithm [89] with radius parameter  $R = 0.8$ . All the jets are required to be in the pseudorapidity interval  $|\eta| < 2.5$  and to have  $p_T > 20$  GeV. All the leptons, both electrons and muons, have  $p_T > 10$  GeV and  $|\eta| < 2.5$ . The missing transverse momenta ( $p_T^{miss}$ ) is calculated from the momentum imbalance along the transverse direction for all the reconstructed objects. As we have mainly focused on the multi-jet final state we did not bother about the isolation requirement of the leptons.

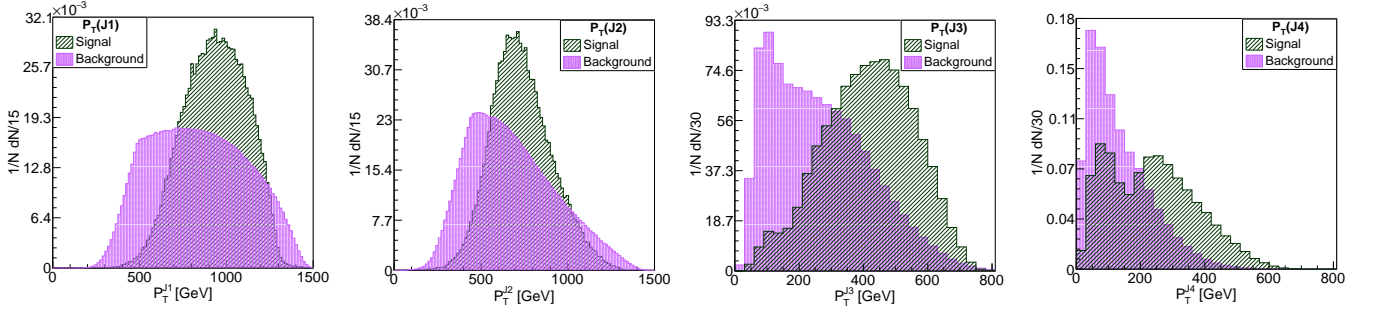


FIG. 5. Normalized  $p_T$  distribution of leading 4-fat-jets for signal (benchmark point  $M_{H^{\pm\pm}} = 1$  TeV) at 3 TeV  $\mu^+\mu^-$  collider.

### 1. Cut based analysis

After reconstruction of all the physical objects (mostly jets), we then follow the cut and count method to discriminate our signal from the background. The cut flow for two benchmark mass points,  $M_{H^{\pm\pm}} = 1000$  GeV and

$M_{H^{\pm\pm}} = 1400$  GeV are given in Table I. From Fig. 5 it can be seen that the 4th jet is quite soft. Hence imposing a hard cut on all the reconstructed 4 fat-jets, we found it more effective to put large  $p_T$  cuts on the leading jets and a relaxed  $p_T$  cut on the sub-leading ones.

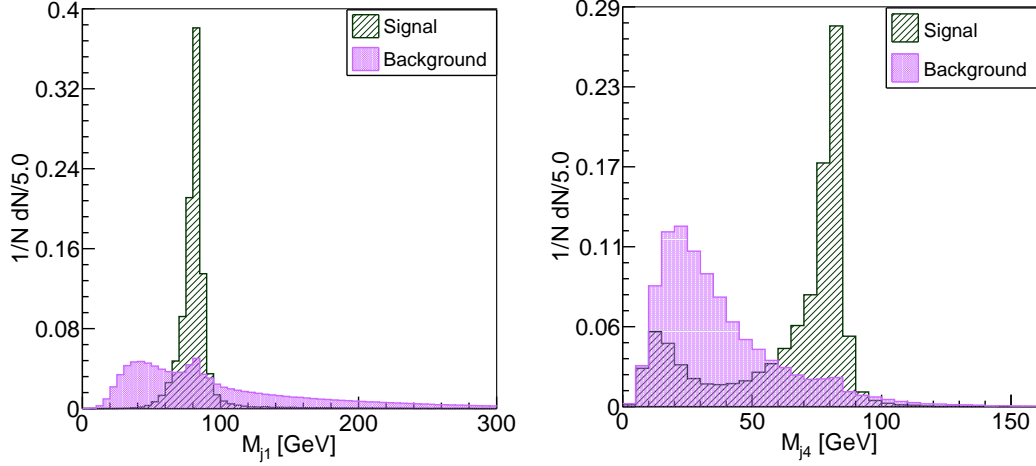


FIG. 6. Normalized invariant mass distribution of  $j_1$  and  $j_4$  for signal ( $M_{H^{\pm\pm}} = 1$  TeV) and background at 3 TeV center of mass energy of  $\mu^+\mu^-$  collider.

In Fig. 6, we plot the invariant mass of  $j_1$  ( $M_{j1}$ ) and  $j_4$  ( $M_{j4}$ ) out of the leading 4 fat-jets. The distribution of  $M_{j1}$  and  $M_{j4}$  shows a clear peak around  $M_{W^\pm}$ . From this it is clear that the two prong W-jet submerged to form a single fat-jets. The small peak of  $M_{j4}$  distribution signifies that the low  $p_T$  jets are not pure W-jet. We also tried to reconstruct the invariant mass of the doubly-charged scalars ( $H^{\pm\pm}$ ), out of the final state sig-

nal fat-jets. In Fig. 7, we plot the two invariant mass reconstructed out of the final state fat-jets.  $M_{jj}^1$  and  $M_{jj}^2$  are the first and second pair of reconstructed invariant mass out of the four final fat-jets respectively. During the selection process of the second pair, we remove the those fat-jets which are already considered in construction the first pair, which takes care of the double counting. As we have shown the distribution for our



benchmark point,  $M_{H^{\pm\pm}} = 1000$  GeV, we can see the invariant mass distributions clearly peaks around 1000 GeV for signal process.

To discriminate the signal from the background, we select events within 20 GeV mass window ( $|M_{W^\pm} - M_{ji}| =$

$\Delta M_{ji} < 20$  GeV) around  $M_{W^\pm}$  for the leading three fat-jets. We also select events lying within a 100 GeV mass gap around the mass of  $H^{\pm\pm}$  ( $|M_{H^{\pm\pm}} - M_{jj}^i| = \Delta M_{jj}^i < 100$  GeV) to reduce the background further. We have summarized the results in cut flow Table. I.

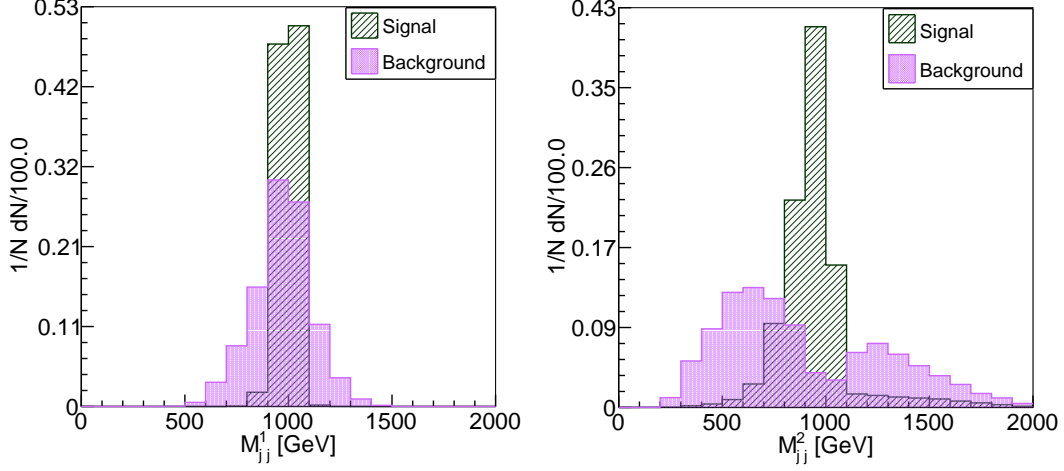


FIG. 7. Normalized invariant mass distribution  $M_{jj}^1$  (first pair) and  $M_{jj}^2$  (second pair) for signal ( $M_{H^{\pm\pm}} = 1$  TeV) and background at 3 TeV  $\mu^+\mu^-$  collider.

## 2. Cut-based Results

With the optimized signal and background events, that survive the selection cuts, we analyse the signal sensitivity. With  $s$  and  $b$  being the signal cross section and background cross section after all the selection cuts, the statistical significance is defined as [90, 91]

$$\sigma_{dis} = \left[ 2 \left( (s+b) \ln \left[ 1 + \frac{s}{b} \right] - s \right) \right]^{1/2} \quad (14)$$

For a  $5\sigma$  discovery we assume  $\sigma_{dis} \geq 5$ . The luminosity required for  $5\sigma$  discovery for different benchmark mass of doubly charged scalar have been shown in Fig. 8.

## 3. Multivariate Analysis (MVA)

In this section we discuss the results of the multivariate analysis (MVA) [92] that we have performed. Fig. 11 shows the kinematic variables used for the MVA analysis assuming the variables are having a good discriminating power between the signal and background, and have low correlations among themselves. A detailed discus-

sion about the variables used has already been presented in the text. The method-unspecific separation is a good measure of the discriminating power of any variable, for a given feature  $y$  [92]. This is defined as,

$$\langle S^2 \rangle = \frac{1}{2} \int dy \frac{(\hat{y}_S(y) - \hat{y}_B(y))^2}{\hat{y}_S(y) + \hat{y}_B(y)} \quad (15)$$

where  $\hat{y}_S$  and  $\hat{y}_B$  are the probability functions for the signal and background for the particular feature  $y$ . The quantity is equal to zero for similar signal and background distributions, and 1 for distributions with no overlaps. We have considered those variables having method-unspecific separation value greater than 1%. In Table. II, we present the method-unspecific separation for the input variables. In Fig. 9, we have shown the Pearson's linear correlation coefficients between the input variables, defined as,

$$\rho(x, y) = \frac{\langle xy \rangle - \langle x \rangle \langle y \rangle}{\sigma_x \sigma_y} \quad (16)$$

where  $\langle x \rangle$  and  $\sigma_x$  are the expectation value and standard deviation respectively for the dataset  $x$ .

$\mu^+\mu^- \rightarrow H^{++}H^{--} \rightarrow W^+W^+W^-W^- \rightarrow Nj_{\text{fat}}$										
$M_{H^{\pm\pm}}$ (GeV)	$\geq 4j$	$p_T^{j1} > 450$	$p_T^{j2} > 350$	$p_T^{j3} > 200$	$p_T^{j4} > 100$	$\Delta M_{j1} < 20$	$\Delta M_{j2} < 20$	$\Delta M_{j3} < 20$	$\Delta M_{jj}^1 < 100$	$\Delta M_{jj}^2 < 100$
1000 [0.825]	0.739	0.736	0.730	0.679	0.540	0.504	0.442	0.388	0.380	0.220
1400 [0.0922]	0.064	0.0623	0.062	0.060	0.053	0.050	0.046	0.041	0.039	0.019
Backgrounds										
BG	$\geq 4j$	$p_T^{j1} > 450$	$p_T^{j2} > 350$	$p_T^{j3} > 200$	$p_T^{j4} > 100$	$\Delta M_{j1} < 20$	$\Delta M_{j2} < 20$	$\Delta M_{j3} < 20$	$\Delta M_{jj}^1 < 100$	$\Delta M_{jj}^2 < 100$
$VV + 2j$ [4.680]	1.527	1.390	1.256	0.351	0.156	0.066	0.028	0.0092	0.0053	0.0005
$V + 3j$ [5.450]	3.613	3.319	3.077	1.815	0.907	0.284	0.088	0.0265	0.0151	0.002
$4j$ [6.677]	5.123	4.830	4.560	3.038	1.840	0.448	0.113	0.0288	0.0163	0.0019
$V + 2j$ [5.360]	1.787	1.669	1.554	1.055	0.486	0.185	0.063	0.0195	0.0109	0.0013
$VVV + 2j$ [0.049]	0.048	0.034	0.027	0.021	0.015	0.0036	0.002	0.0017	0.001	0.00009

TABLE I. The cut-flow for the signal and backgrounds. For signal two benchmark  $M_{H^{\pm\pm}} = 1000$  GeV and  $M_{H^{\pm\pm}} = 1400$  GeV are considered. The values mentioned in square brackets are the production cross section of each processes. The cross sections are in fb.

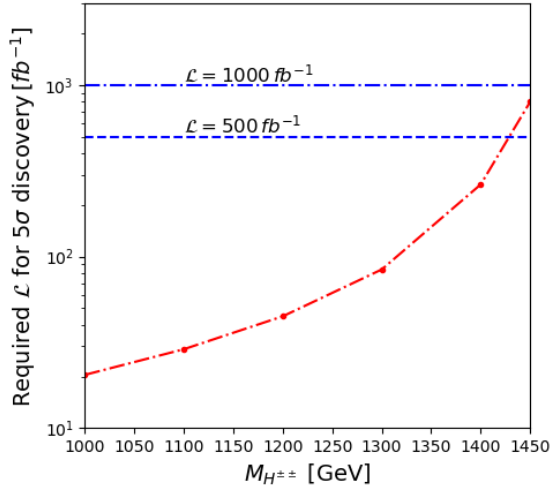


FIG. 8. Required luminosity for  $5\sigma$  discovery of the doubly-charged scalars at 3 TeV  $\mu^+\mu^-$  collider.

We present the BDT response and cut efficiency at a benchmark mass value,  $M_{H^{\pm\pm}} = 1000$  GeV, in Fig. 10. We have used the optimised hyperparameters at different

In Table. III, we have summarised the relevant BDT hyperparameters. We have optimised the BDT hyperparameters with *adaptive boost* algorithm with a learning rate of 0.1. The so-called *Gini index* has been used for the separation between the nodes in decision trees. In Table. II, we also present the method-specific ranking of the input variables, which shows the importance of the used variables in separating signal from background.

benchmark mass to obtain the statistical significance,

$$\mathcal{Z} = \frac{N_S}{\sqrt{N_S + N_B}} \quad (17)$$

where  $N_S$  and  $N_B$  are the number of signal and background events after the optimal cut is applied on the BDT response. In Table. IV, we present the obtained statistical significance  $\mathcal{Z}$  for different benchmark doubly-charged scalar mass  $M_{H^{\pm\pm}}$ .

#### IV. SUMMARY

We have discussed the discovery prospects of the doubly-charged scalar,  $H^{\pm\pm}$ , present in Type-II seesaw

model in  $\mu^+\mu^-$  collider. We mainly focus our attention to that part of the parameter space where the produced



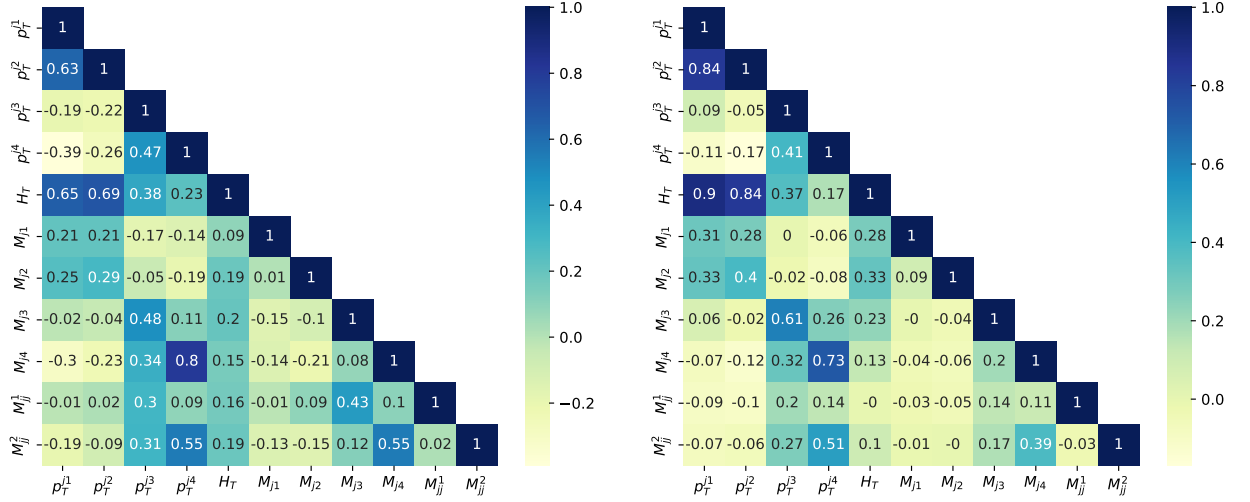


FIG. 9. The linear correlation coefficients for signal (left) and background (right) between the different kinematic variables used in multivariate analysis.

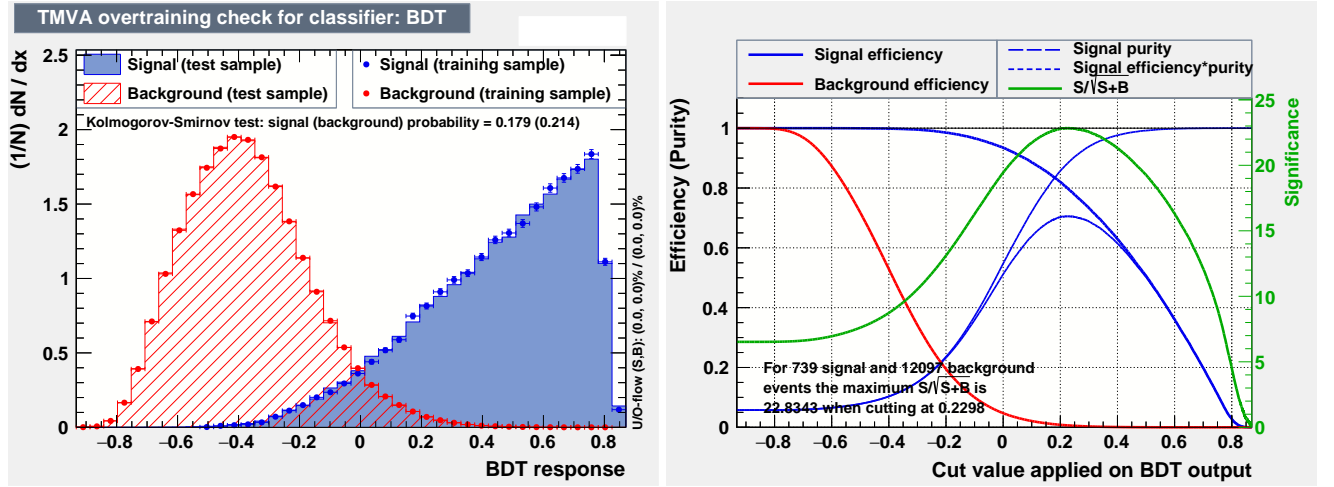


FIG. 10. (Left): Normalised distribution of the BDT response for both signal(blue) and background(red) classes (both training and testing samples). (Right): Signal(blue) and background(red) efficiencies along with the statistical significance(green) of the signal as function of applied BDT cut value.

doubly-charged scalar mainly decays into  $W^\pm W^\pm$  final state and subsequently we consider the hadronic final states from the  $W$  decays. All hadronic final states are not favourable channel to probe at the LHC due to the presence of the towering QCD backgrounds. Hence this region is more favorable for linear colliders, *viz*  $e^+e^-$  and  $\mu^+\mu^-$  collider. Among these two, the  $\mu^+\mu^-$  collider has a low energy loss due to synchrotron radiation. Firstly, we have performed the trivial cut-based analysis and predict the statistical significance of the muon collider at  $\sqrt{s} = 3$  TeV. Secondly, we have also performed a multivariate analysis and compared both the results. From the cut-

based analysis we have concluded that at  $1000 \text{ fb}^{-1}$  luminosity up to 1450 GeV massive doubly-charged scalar can be discovered with  $5\sigma$  confidence level, see Fig. 8. The result from the multivariate analysis for different  $M_H^{\pm\pm}$  value has been given in Table. IV, from which it is evident that, apart from a higher mass of 1.450 TeV, BDT analysis offers a larger statistical significance, greater than  $5\sigma$ .

Feature	Method-unspecific separation	Method-specific ranking
$M_{j3}$	0.393	0.144
$M_{j1}$	0.391	0.142
$M_{jj}^2$	0.384	0.102
$M_{jj}^1$	0.336	0.095
$M_{j2}$	0.289	0.116
$M_{j4}$	0.257	0.096
$p_T^{j3}$	0.241	0.063
$p_T^{j4}$	0.229	0.045
$H_T$	0.218	0.066
$p_T^{j1}$	0.141	0.057
$p_T^{j2}$	0.137	0.069

TABLE II. Method unspecific and Method specific relative importance of the different discriminating variables used in MVA.

BDT hyperparameter	Optimised choice
NTrees	500
MinNodeSize	5.0%
MaxDepth	5
BoostType	AdaBoost
AdaBoostBeta	0.1
UseBaggedBoost	True
BaggedSampleFraction	0.5
SeparationType	GiniIndex
nCuts	20

TABLE III. Summary of optimised BDT hyperparameters.

Mass[GeV]	Significance
1000	22.834
1100	19.303
1200	15.256
1300	10.959
1400	6.259
1450	3.640

TABLE IV. Statistical significance,  $\mathcal{Z}$ , for different doubly-charged scalar mass obtained from the multivariate analysis for muon collider with center of mass  $\sqrt{s} = 3$  TeV and integrated luminosity  $\mathcal{L} = 1000 \text{ fb}^{-1}$ .

## V. ACKNOWLEDGMENTS

The authors acknowledge SAMKHYA: high Performance Computing Facility provided by Institute of physics, for the performed simulations. The authors acknowledge the support from the Indo-French Centre for

the Promotion of Advanced Research (Grant no: 6304-2). SPM thank Saiyad Ashanujjaman, Rojalin Padhan and Agnivo Sarkar for the useful discussions.

## REFERENCES

- [1] S. Weinberg, Baryon and Lepton Nonconserving Processes, *Phys. Rev. Lett.* **43**, 1566 (1979).
- [2] P. Minkowski,  $\mu \rightarrow e\gamma$  at a Rate of One Out of  $10^9$  Muon Decays?, *Phys. Lett. B* **67**, 421 (1977).
- [3] M. Gell-Mann, P. Ramond, and R. Slansky, Complex Spinors and Unified Theories, *Conf. Proc. C* **790927**, 315 (1979), [arXiv:1306.4669 \[hep-th\]](#).
- [4] R. N. Mohapatra and G. Senjanovic, Neutrino Mass and Spontaneous Parity Nonconservation, *Phys. Rev. Lett.* **44**, 912 (1980).
- [5] J. Schechter and J. W. F. Valle, Neutrino Masses in  $SU(2) \times U(1)$  Theories, *Phys. Rev. D* **22**, 2227 (1980).
- [6] T. P. Cheng and L.-F. Li, Neutrino Masses, Mixings and Oscillations in  $SU(2) \times U(1)$  Models of Electroweak Interactions, *Phys. Rev. D* **22**, 2860 (1980).
- [7] R. N. Mohapatra and G. Senjanovic, Neutrino Masses and Mixings in Gauge Models with Spontaneous Parity Violation, *Phys. Rev. D* **23**, 165 (1981).
- [8] R. Foot, H. Lew, X. G. He, and G. C. Joshi, Seesaw Neutrino Masses Induced by a Triplet of Leptons, *Z. Phys. C* **44**, 441 (1989).
- [9] A. Melfo, M. Nemevsek, F. Nesti, G. Senjanovic, and Y. Zhang, Type II Seesaw at LHC: The Roadmap, *Phys. Rev. D* **85**, 055018 (2012), [arXiv:1108.4416 \[hep-ph\]](#).
- [10] K. Huitu, J. Maalampi, A. Pietila, and M. Raidal, Doubly charged Higgs at LHC, *Nucl. Phys. B* **487**, 27 (1997), [arXiv:hep-ph/9606311](#).
- [11] J. F. Gunion, C. Loomis, and K. T. Pitts, Searching for doubly charged Higgs bosons at future colliders, *eConf C960625*, LTH096 (1996), [arXiv:hep-ph/9610237](#).
- [12] S. Chakrabarti, D. Choudhury, R. M. Godbole, and B. Mukhopadhyaya, Observing doubly charged Higgs bosons in photon-photon collisions, *Phys. Lett. B* **434**, 347 (1998), [arXiv:hep-ph/9804297](#).
- [13] M. Muhlleitner and M. Spira, A Note on doubly charged Higgs pair production at hadron colliders, *Phys. Rev. D* **68**, 117701 (2003), [arXiv:hep-ph/0305288](#).
- [14] A. G. Akeroyd and M. Aoki, Single and pair production of doubly charged Higgs bosons at hadron colliders, *Phys. Rev. D* **72**, 035011 (2005), [arXiv:hep-ph/0506176](#).
- [15] T. Han, B. Mukhopadhyaya, Z. Si, and K. Wang, Pair production of doubly-charged scalars: Neutrino mass constraints and signals at the LHC, *Phys. Rev. D* **76**, 075013 (2007), [arXiv:0706.0441 \[hep-ph\]](#).

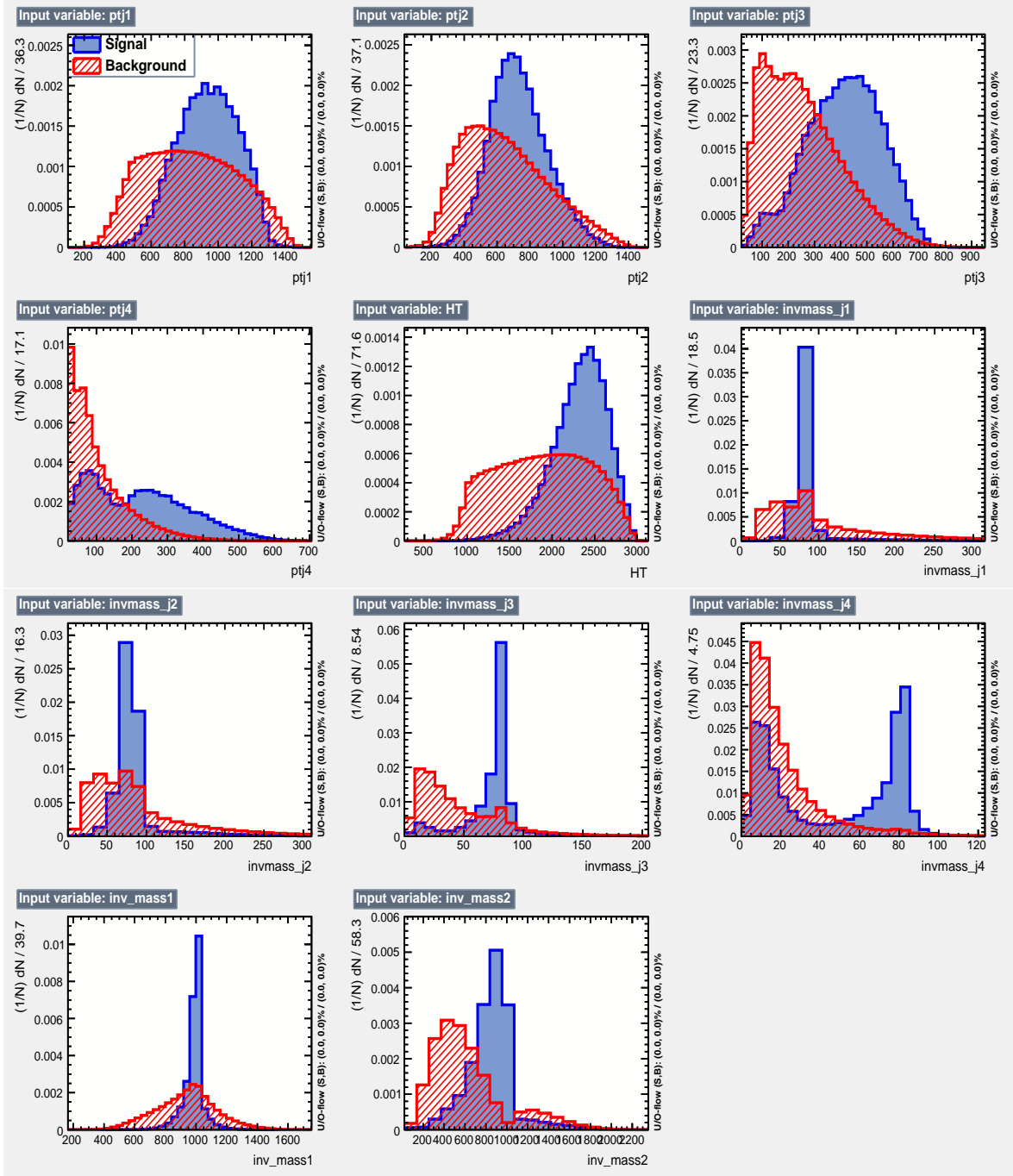


FIG. 11. Distributions of different kinematic variables used for MVA for signal as well as for all back grounds. The normalised distributions for signal is given by the solid blue line and the back ground distributions are given by solid red line.

- [16] F. del Aguila and J. A. Aguilar-Saavedra, Distinguishing seesaw models at LHC with multi-lepton signals, *Nucl. Phys. B* **813**, 22 (2009), [arXiv:0808.2468 \[hep-ph\]](#).
- [17] P. Fileviez Perez, T. Han, G.-y. Huang, T. Li, and K. Wang, Neutrino Masses and the CERN LHC: Testing Type II Seesaw, *Phys. Rev. D* **78**, 015018 (2008), [arXiv:0805.3536 \[hep-ph\]](#).
- [18] A. G. Akeroyd and C.-W. Chiang, Doubly charged Higgs bosons and three-lepton signatures in the Higgs Triplet Model, *Phys. Rev. D* **80**, 113010 (2009), [arXiv:0909.4419 \[hep-ph\]](#).
- [19] A. G. Akeroyd, C.-W. Chiang, and N. Gaur, Leptonic signatures of doubly charged Higgs boson production at the LHC, *JHEP* **11**, 005, [arXiv:1009.2780 \[hep-ph\]](#).

- [20] M. Aoki, S. Kanemura, and K. Yagyu, Testing the Higgs triplet model with the mass difference at the LHC, *Phys. Rev. D* **85**, 055007 (2012), [arXiv:1110.4625 \[hep-ph\]](#).
- [21] A. G. Akeroyd and H. Sugiyama, Production of doubly charged scalars from the decay of singly charged scalars in the Higgs Triplet Model, *Phys. Rev. D* **84**, 035010 (2011), [arXiv:1105.2209 \[hep-ph\]](#).
- [22] C.-W. Chiang, T. Nomura, and K. Tsumura, Search for doubly charged Higgs bosons using the same-sign diboson mode at the LHC, *Phys. Rev. D* **85**, 095023 (2012), [arXiv:1202.2014 \[hep-ph\]](#).
- [23] A. G. Akeroyd, S. Moretti, and H. Sugiyama, Five-lepton and six-lepton signatures from production of neutral triplet scalars in the Higgs Triplet Model, *Phys. Rev. D* **85**, 055026 (2012), [arXiv:1201.5047 \[hep-ph\]](#).
- [24] E. J. Chun and P. Sharma, Same-Sign Tetra-Leptons from Type II Seesaw, *JHEP* **08**, 162, [arXiv:1206.6278 \[hep-ph\]](#).
- [25] F. del Águila and M. Chala, LHC bounds on Lepton Number Violation mediated by doubly and singly-charged scalars, *JHEP* **03**, 027, [arXiv:1311.1510 \[hep-ph\]](#).
- [26] E. J. Chun and P. Sharma, Search for a doubly-charged boson in four lepton final states in type II seesaw, *Phys. Lett. B* **728**, 256 (2014), [arXiv:1309.6888 \[hep-ph\]](#).
- [27] S. Kanemura, K. Yagyu, and H. Yokoya, First constraint on the mass of doubly-charged Higgs bosons in the same-sign diboson decay scenario at the LHC, *Phys. Lett. B* **726**, 316 (2013), [arXiv:1305.2383 \[hep-ph\]](#).
- [28] S. Kanemura, M. Kikuchi, K. Yagyu, and H. Yokoya, Bounds on the mass of doubly-charged Higgs bosons in the same-sign diboson decay scenario, *Phys. Rev. D* **90**, 115018 (2014), [arXiv:1407.6547 \[hep-ph\]](#).
- [29] S. Kanemura, M. Kikuchi, H. Yokoya, and K. Yagyu, LHC Run-I constraint on the mass of doubly charged Higgs bosons in the same-sign diboson decay scenario, *PTEP* **2015**, 051B02 (2015), [arXiv:1412.7603 \[hep-ph\]](#).
- [30] Z. Kang, J. Li, T. Li, Y. Liu, and G.-Z. Ning, Light Doubly Charged Higgs Boson via the  $WW^*$  Channel at LHC, *Eur. Phys. J. C* **75**, 574 (2015), [arXiv:1404.5207 \[hep-ph\]](#).
- [31] Z.-L. Han, R. Ding, and Y. Liao, LHC Phenomenology of Type II Seesaw: Nondegenerate Case, *Phys. Rev. D* **91**, 093006 (2015), [arXiv:1502.05242 \[hep-ph\]](#).
- [32] Z.-L. Han, R. Ding, and Y. Liao, LHC phenomenology of the type II seesaw mechanism: Observability of neutral scalars in the nondegenerate case, *Phys. Rev. D* **92**, 033014 (2015), [arXiv:1506.08996 \[hep-ph\]](#).
- [33] M. Mitra, S. Niyogi, and M. Spannowsky, Type-II Seesaw Model and Multilepton Signatures at Hadron Colliders, *Phys. Rev. D* **95**, 035042 (2017), [arXiv:1611.09594 \[hep-ph\]](#).
- [34] D. K. Ghosh, N. Ghosh, I. Saha, and A. Shaw, Revisiting the high-scale validity of the type II seesaw model with novel LHC signature, *Phys. Rev. D* **97**, 115022 (2018), [arXiv:1711.06062 \[hep-ph\]](#).
- [35] S. Antusch, O. Fischer, A. Hammad, and C. Scherb, Low scale type II seesaw: Present constraints and prospects for displaced vertex searches, *JHEP* **02**, 157, [arXiv:1811.03476 \[hep-ph\]](#).
- [36] P. S. Bhupal Dev and Y. Zhang, Displaced vertex signatures of doubly charged scalars in the type-II seesaw and its left-right extensions, *JHEP* **10**, 199, [arXiv:1808.00943 \[hep-ph\]](#).
- [37] T. B. de Melo, F. S. Queiroz, and Y. Villamizar, Doubly Charged Scalar at the High-Luminosity and High-Energy LHC, *Int. J. Mod. Phys. A* **34**, 1950157 (2019), [arXiv:1909.07429 \[hep-ph\]](#).
- [38] R. Primulando, J. Julio, and P. Uttayarat, Scalar phenomenology in type-II seesaw model, *JHEP* **08**, 024, [arXiv:1903.02493 \[hep-ph\]](#).
- [39] E. J. Chun, S. Khan, S. Mandal, M. Mitra, and S. Shil, Same-sign tetralepton signature at the Large Hadron Collider and a future  $pp$  collider, *Phys. Rev. D* **101**, 075008 (2020), [arXiv:1911.00971 \[hep-ph\]](#).
- [40] R. Padhan, D. Das, M. Mitra, and A. Kumar Nayak, Probing doubly and singly charged Higgs bosons at the  $pp$  collider HE-LHC, *Phys. Rev. D* **101**, 075050 (2020), [arXiv:1909.10495 \[hep-ph\]](#).
- [41] S. Ashanujjaman and K. Ghosh, Revisiting type-II seesaw: present limits and future prospects at LHC, *JHEP* **03**, 195, [arXiv:2108.10952 \[hep-ph\]](#).
- [42] S. Ashanujjaman, K. Ghosh, and R. Sahu, Low-mass doubly charged Higgs bosons at the LHC, *Phys. Rev. D* **107**, 015018 (2023), [arXiv:2211.00632 \[hep-ph\]](#).
- [43] T. Nomura, H. Okada, and H. Yokoya, Discriminating leptonic Yukawa interactions with doubly charged scalar at the ILC, *Nucl. Phys. B* **929**, 193 (2018), [arXiv:1702.03396 \[hep-ph\]](#).
- [44] S. Blunier, G. Cottin, M. A. Díaz, and B. Koch, Phenomenology of a Higgs triplet model at future  $e^+e^-$  colliders, *Phys. Rev. D* **95**, 075038 (2017), [arXiv:1611.07896 \[hep-ph\]](#).
- [45] A. Crivellin, M. Ghezzi, L. Panizzi, G. M. Pruna, and A. Signer, Low- and high-energy phenomenology of a doubly charged scalar, *Phys. Rev. D* **99**, 035004 (2019), [arXiv:1807.10224 \[hep-ph\]](#).
- [46] P. Agrawal, M. Mitra, S. Niyogi, S. Shil, and M. Spannowsky, Probing the Type-II Seesaw Mechanism through the Production of Higgs Bosons at a Lepton Collider, *Phys. Rev. D* **98**, 015024 (2018), [arXiv:1803.00677 \[hep-ph\]](#).
- [47] L. Rahili, A. Arhrib, and R. Benbrik, Associated production of SM Higgs with a photon in type-II seesaw

- models at the ILC, *Eur. Phys. J. C* **79**, 940 (2019), [arXiv:1909.07793 \[hep-ph\]](#).
- [48] S. Ashanujjaman, K. Ghosh, and K. Huitu, Type-II seesaw: searching the LHC elusive low-mass triplet-like Higgses at  $e^-e^+$  colliders, (2022), [arXiv:2205.14983 \[hep-ph\]](#).
- [49] P. S. B. Dev, S. Khan, M. Mitra, and S. K. Rai, Doubly-charged Higgs boson at a future electron-proton collider, *Phys. Rev. D* **99**, 115015 (2019), [arXiv:1903.01431 \[hep-ph\]](#).
- [50] X.-H. Yang and Z.-J. Yang, Doubly charged Higgs production at future ep colliders \*, *Chin. Phys. C* **46**, 063107 (2022), [arXiv:2103.11412 \[hep-ph\]](#).
- [51] Y. Cai, T. Han, T. Li, and R. Ruiz, Lepton Number Violation: Seesaw Models and Their Collider Tests, *Front. in Phys.* **6**, 40 (2018), [arXiv:1711.02180 \[hep-ph\]](#).
- [52] F. F. Deppisch, P. S. Bhupal Dev, and A. Pilaftsis, Neutrinos and Collider Physics, *New J. Phys.* **17**, 075019 (2015), [arXiv:1502.06541 \[hep-ph\]](#).
- [53] G. Aad et al. (ATLAS), Search for doubly-charged Higgs bosons in like-sign dilepton final states at  $\sqrt{s} = 7$  TeV with the ATLAS detector, *Eur. Phys. J. C* **72**, 2244 (2012), [arXiv:1210.5070 \[hep-ex\]](#).
- [54] S. Chatrchyan et al. (CMS), A Search for a Doubly-Charged Higgs Boson in  $pp$  Collisions at  $\sqrt{s} = 7$  TeV, *Eur. Phys. J. C* **72**, 2189 (2012), [arXiv:1207.2666 \[hep-ex\]](#).
- [55] G. Aad et al. (ATLAS), Search for anomalous production of prompt same-sign lepton pairs and pair-produced doubly charged Higgs bosons with  $\sqrt{s} = 8$  TeV  $pp$  collisions using the ATLAS detector, *JHEP* **03**, 041, [arXiv:1412.0237 \[hep-ex\]](#).
- [56] G. Aad et al. (ATLAS), Search for new phenomena in events with three or more charged leptons in  $pp$  collisions at  $\sqrt{s} = 8$  TeV with the ATLAS detector, *JHEP* **08**, 138, [arXiv:1411.2921 \[hep-ex\]](#).
- [57] Search for a doubly-charged Higgs boson with  $\sqrt{s} = 8$  TeV  $pp$  collisions at the CMS experiment, (2016).
- [58] M. Aaboud et al. (ATLAS), Search for doubly charged Higgs boson production in multi-lepton final states with the ATLAS detector using proton-proton collisions at  $\sqrt{s} = 13$  TeV, *Eur. Phys. J. C* **78**, 199 (2018), [arXiv:1710.09748 \[hep-ex\]](#).
- [59] A. M. Sirunyan et al. (CMS), Observation of electroweak production of same-sign W boson pairs in the two jet and two same-sign lepton final state in proton-proton collisions at  $\sqrt{s} = 13$  TeV, *Phys. Rev. Lett.* **120**, 081801 (2018), [arXiv:1709.05822 \[hep-ex\]](#).
- [60] A search for doubly-charged Higgs boson production in three and four lepton final states at  $\sqrt{s} = 13$  TeV, (2017).
- [61] M. Aaboud et al. (ATLAS), Search for doubly charged scalar bosons decaying into same-sign W boson pairs with the ATLAS detector, *Eur. Phys. J. C* **79**, 58 (2019), [arXiv:1808.01899 \[hep-ex\]](#).
- [62] G. Aad et al. (ATLAS), Search for doubly and singly charged Higgs bosons decaying into vector bosons in multi-lepton final states with the ATLAS detector using proton-proton collisions at  $\sqrt{s} = 13$  TeV, *JHEP* **06**, 146, [arXiv:2101.11961 \[hep-ex\]](#).
- [63] Search for doubly charged Higgs boson production in multi-lepton final states using 139 fb $^{-1}$  of proton-proton collisions at  $\sqrt{s} = 13$  TeV with the ATLAS detector, (2022).
- [64] The International Linear Collider Technical Design Report - Volume 1: Executive Summary, (2013), [arXiv:1306.6327 \[physics.acc-ph\]](#).
- [65] CEPC Conceptual Design Report: Volume 1 - Accelerator, (2018), [arXiv:1809.00285 \[physics.acc-ph\]](#).
- [66] CERN FCC webpage, .
- [67] Compact Linear Collider (CLIC) webpage, .
- [68] R. Palmer et al., Muon collider design, *Nucl. Phys. B Proc. Suppl.* **51**, 61 (1996), [arXiv:acc-phys/9604001](#).
- [69] C. M. Ankenbrandt et al., Status of muon collider research and development and future plans, *Phys. Rev. ST Accel. Beams* **2**, 081001 (1999), [arXiv:physics/9901022](#).
- [70] J. P. Delahaye, M. Diemoz, K. Long, B. Mansoulié, N. Pastrone, L. Rivkin, D. Schulte, A. Skrinsky, and A. Wulzer, Muon Colliders, (2019), [arXiv:1901.06150 \[physics.acc-ph\]](#).
- [71] K. Long, D. Lucchesi, M. Palmer, N. Pastrone, D. Schulte, and V. Shiltsev, Muon colliders to expand frontiers of particle physics, *Nature Phys.* **17**, 289 (2021), [arXiv:2007.15684 \[physics.acc-ph\]](#).
- [72] H. Al Ali et al., The muon Smasher's guide, *Rept. Prog. Phys.* **85**, 084201 (2022), [arXiv:2103.14043 \[hep-ph\]](#).
- [73] A. Costantini, F. De Lillo, F. Maltoni, L. Mantani, O. Mattelaer, R. Ruiz, and X. Zhao, Vector boson fusion at multi-TeV muon colliders, *JHEP* **09**, 080, [arXiv:2005.10289 \[hep-ph\]](#).
- [74] P. Bandyopadhyay, A. Karan, and C. Sen, Discerning Signatures of Seesaw Models and Complementarity of Leptonic Colliders, (2020), [arXiv:2011.04191 \[hep-ph\]](#).
- [75] T. Han, Y. Ma, and K. Xie, High energy leptonic collisions and electroweak parton distribution functions, *Phys. Rev. D* **103**, L031301 (2021), [arXiv:2007.14300 \[hep-ph\]](#).
- [76] A. Arhrib, R. Benbrik, M. Chabab, G. Moulhaka, M. C. Peyranere, L. Rahili, and J. Ramadan, The Higgs Potential in the Type II Seesaw Model, *Phys. Rev. D* **84**, 095005 (2011), [arXiv:1105.1925 \[hep-ph\]](#).
- [77] P. A. Zyla et al. (Particle Data Group), Review of Particle Physics, *PTEP* **2020**, 083C01 (2020).

- [78] M. Kakizaki, Y. Ogura, and F. Shima, Lepton flavor violation in the triplet Higgs model, *Phys. Lett. B* **566**, 210 (2003), [arXiv:hep-ph/0304254](#).
- [79] D. N. Dinh, A. Ibarra, E. Molinaro, and S. T. Petcov, The  $\mu - e$  Conversion in Nuclei,  $\mu \rightarrow e\gamma$ ,  $\mu \rightarrow 3e$  Decays and TeV Scale See-Saw Scenarios of Neutrino Mass Generation, *JHEP* **08**, 125, [Erratum: JHEP 09, 023 (2013)], [arXiv:1205.4671 \[hep-ph\]](#).
- [80] A. M. Baldini *et al.* (MEG), Search for the lepton flavour violating decay  $\mu^+ \rightarrow e^+\gamma$  with the full dataset of the MEG experiment, *Eur. Phys. J. C* **76**, 434 (2016), [arXiv:1605.05081 \[hep-ex\]](#).
- [81] U. Bellgardt *et al.* (SINDRUM), Search for the Decay  $\mu^+ \rightarrow e^+ e^+ e^-$ , *Nucl. Phys. B* **299**, 1 (1988).
- [82] T. G. Rizzo, Decays of Heavy Higgs Bosons, *Phys. Rev. D* **22**, 722 (1980).
- [83] W.-Y. Keung and W. J. Marciano, HIGGS SCALAR DECAYS:  $H \rightarrow W^+ X$ , *Phys. Rev. D* **30**, 248 (1984).
- [84] A. M. Sirunyan *et al.* (CMS), Search for physics beyond the standard model in multilepton final states in proton-proton collisions at  $\sqrt{s} = 13$  TeV, *JHEP* **03**, 051, [arXiv:1911.04968 \[hep-ex\]](#).
- [85] J. Alwall, R. Frederix, S. Frixione, V. Hirschi, F. Maltoni, O. Mattelaer, H. S. Shao, T. Stelzer, P. Torrielli, and M. Zaro, The automated computation of tree-level and next-to-leading order differential cross sections, and their matching to parton shower simulations, *JHEP* **07**, 079, [arXiv:1405.0301 \[hep-ph\]](#).
- [86] T. Sjöstrand, S. Ask, J. R. Christiansen, R. Corke, N. Desai, P. Ilten, S. Mrenna, S. Prestel, C. O. Rasmussen, and P. Z. Skands, An introduction to PYTHIA 8.2, *Comput. Phys. Commun.* **191**, 159 (2015), [arXiv:1410.3012 \[hep-ph\]](#).
- [87] J. de Favereau, C. Delaere, P. Demin, A. Giammanco, V. Lemaitre, A. Mertens, and M. Selvaggi (DELPHES 3), DELPHES 3, A modular framework for fast simulation of a generic collider experiment, *JHEP* **02**, 057, [arXiv:1307.6346 \[hep-ex\]](#).
- [88] M. Cacciari, G. P. Salam, and G. Soyez, FastJet User Manual, *Eur. Phys. J. C* **72**, 1896 (2012), [arXiv:1111.6097 \[hep-ph\]](#).
- [89] Y. L. Dokshitzer, G. D. Leder, S. Moretti, and B. R. Webber, Better jet clustering algorithms, *JHEP* **08**, 001, [arXiv:hep-ph/9707323](#).
- [90] G. Cowan, K. Cranmer, E. Gross, and O. Vitells, Asymptotic formulae for likelihood-based tests of new physics, *Eur. Phys. J. C* **71**, 1554 (2011), [Erratum: Eur.Phys.J.C 73, 2501 (2013)], [arXiv:1007.1727 \[physics.data-an\]](#).
- [91] G. Cowan, Two developments in discovery tests: use of weighted Monte Carlo events and an improved measure of experimental sensitivity, .
- [92] A. Hocker *et al.*, TMVA - Toolkit for Multivariate Data Analysis, (2007), [arXiv:physics/0703039](#).